Available online at www.sciencedirect.com
SCIENCE DIRECT®
Physics Letters A 340 (2005) 220–227
PHYSICS LETTERS A
www.elsevier.com/locate/pla

Size and phonon-confinement effects on low-frequency Raman mode of anatase TiO_2 nanocrystal

Ke-Rong Zhu [a,b], Ming-Sheng Zhang [a,*], Qiang Chen [a], Zhen Yin [a]

[a] *National Laboratory of Solid State Microstructures and Center for Materials Analysis, Nanjing University, Nanjing 210093, People's Republic of China*
[b] *School of Physics & Material Science and Center of Modern Experimental Technology, Anhui University, Hefei 230093, People's Republic of China*

Received 20 February 2005; received in revised form 27 March 2005; accepted 4 April 2005

Available online 13 April 2005

Communicated by B. Fricke

Abstract

Raman spectra of anatase TiO_2 nanocrystals with 2.2–25.5 nm grain sizes were measured at temperature range 83–293 K. The size dependences of the frequency, the bandwidth and the lineshape of the low-frequency mode agree well with those calculated on the basis of the phonon confinement model with the theoretical phonon dispersion relationships. The correlations of both Raman frequency and bandwidth to the grain size L satisfy a $L^{-1.3}$ law. The contributions of three-phonon anharmonic processes to the frequency and bandwidth at various grain sizes were obtained from the temperature dependence of the Raman spectra, and the results show that the phonon coupling is increased in anatase TiO_2 nanocrystal.

PACS: 78.30.-j; 63.22.+m; 63.20.Dj; 63.20.Kr

Keywords: TiO_2 nanocrystal; Raman spectra; Phonon confinement

1. Introduction

Recently anatase titanium dioxide (TiO_2) nanocrystals have been attracted much attention owing to novel physical, chemical and electrical properties for various applications to electrochemical solar cells, rocking-chair lithium batteries, photocatalysis and so on [1–4]. Among three natural phases including rutile and brookite, anatase phase is an important one. Anatase has tetragonal structure of space group D_{4h}^{19} with two formulas per unit cell and thus has six Raman active modes ($A_{1g} + 2B_{1g} + 3E_g$). It was demonstrated that the blueshift and broadening of low-frequency E_g mode (143 cm^{-1}) observed in anatase

* Corresponding author.
E-mail address: mszhang@nju.edu.cn (M.-S. Zhang).

0375-9601/$ – see front matter
doi:10.1016/j.physleta.2005.04.008

TiO_2 nanocrystals prepared with gas condensation technique were related to the oxygen stoichiometry instead of any internal stress or grain size effects [5]. Size-effects on the frequency and bandwidth of the E_g mode in anatase nanocrystals derived from hydrolysis of tetrabutyl titanate and alkoxide were recorded to be ascribed to phonon confinement [6–8]. Besides conventional size-effects on the Raman frequency and bandwidth, size-effect on the phonon–phonon coupling is worthy to be examined. Temperature dependence of the Raman spectra show that phonon–phonon coupling was increased with decreasing the particle size in Si and CdSe nanocrystals [9,10], but was not increased in CeO_2 nanoparticles [11]. The size-effect on the phonon coupling in anatase TiO_2 nanocrystals has not been discussed until now. In this Letter, we present Raman spectra of anatase TiO_2 nanocrystals at temperature range 83–293 K and study in detail the size dependence and temperature dependence of the low-frequency E_g mode. Not only we find an empirical formula for describing the relationship between the particle size and both frequency shift and line width due to phonon confinement, but also we obtain the size dependence of three-phonon anharmonic processes in anatase TiO_2 nanocrystal derived from hydrolysis of tetrabutyl titanate.

2. Experiment details

Titanium dioxide (TiO_2) nanocrystals of anatase phase were synthesized by hydrolysis method [8]. An ethanol solution of tetrabutyl titanate, $Ti(OC_4H_9)_4$, was slowly added into deionized water which was vigorously stirred. The resulting titania gel was washed with deionized water, followed by evaporation in atmosphere at room temperature for a few days. Then as-prepared nanocrystal was annealed in air for 1 h at temperature range 373–923 K. The phase contents, the lattice parameters and the averaged particle size were determined from the X-ray diffraction (XRD). The diffraction patterns were collected using a D/Max-RA diffractionmeter with CuKa radiation in the step-scanning mode.

Raman spectra were measured in the back scattering configuration at the temperature range 83–293 K using JY HR800 Raman spectrometer. The 488 nm line of air-cooled Ar-ion laser was used as an excitation, and the output power was set at 5 mW. The temperature fluctuation of the sample was controlled within ± 1 K by a TMS94 heating/cooling stage.

3. Results and discussion

X-ray diffraction patterns of the TiO_2 nanocrystals are shown in Fig. 1, where standard XRD pattern of anatase, brookite and rutile from JCPDS cards with relatively characteristic peaks are also plotted in order to identify diffraction lines. Annealed at the temperature below 873 K, anatase is main phase in our samples. Brookite content is about 30%wt in the as-prepared sample and decreases to near zero as annealing temperature is up to 773 K, at which rutile phase appears, and then reaches 54%wt as the annealing temperature gets up to 873 K. The averaged anatase grain sizes were determined according to the Scherrer's equation $D = k\lambda/\beta\cos\theta$, where D is the grain size; k is a constant (shape factor, about 0.9);

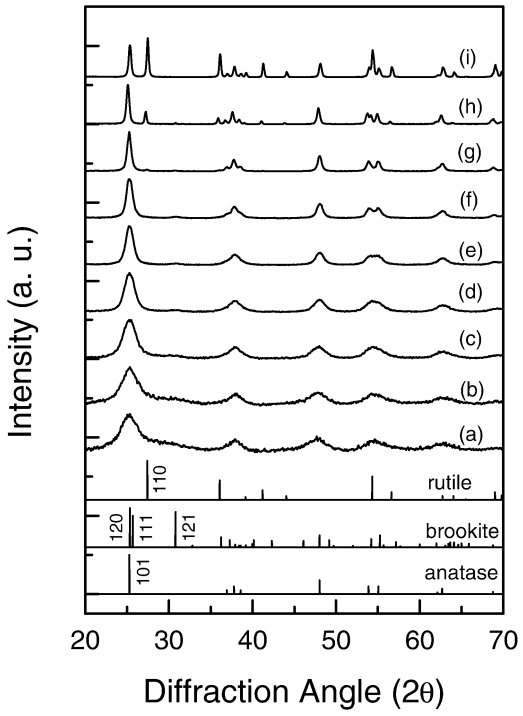

Fig. 1. XRD patterns of the as-prepared (a), and annealed at (b) 373, (c) 473, (d) 573, (e) 673, (f) 723, (g) 773, (h) 823 and (i) 873 K, respectively.

λ is the X-ray wavelength; β is the full width at half maximum of the diffraction line and θ is the diffraction angle. The values of β and θ are from anatase (200) diffraction line. The results show that the averaged sizes are equal to 2.2, 2.5, 3.2, 5.1, 7.8, 12.7, 14.6, 20.4 and 25.5 nm for the as-prepared, and annealed at 373, 473, 573, 673, 723, 773, 823 and 873 K, respectively. However, it should point out that the uncertainty of the calculated particle size really exist, especially in the case of extrafine particle size. The numerical uncertainty for the particle sizes calculated with XRD is within 10% in our case. The lattice parameters of anatase phase in all samples are almost the same, with a of 0.3784 nm and c of 0.9512 nm, in agreement with data in Ref. [12].

Raman spectra from all samples at room temperature are shown in Fig. 2. Raman modes at 144, 196, 396, 516 and 639 cm^{-1} are assigned as E_g, E_g, B_{1g}, A_{1g} (or B_{1g}), and E_g modes in anatase phase, respectively. The 232, 449 and 612 cm^{-1} modes in the 25.5 nm sample come from rutile phase. Although there is a little brookite phase in the smaller size samples, no distinct Raman modes were recorded from brookite phase. The strong backgrounds in the 2.2 and 2.5 nm samples may be from Raman scattering of brookite and amorphous TiO_2 [13,14]. The Raman modes at 143.5, 196.1, 396.1, 516.1 and 639.5 cm^{-1} in the 25.5 nm sample are close to 144, 198, 397, 516 and 639 cm^{-1} in bulk anatase [13], which indicates that phonons in the 25.5 nm sample have the same characters with that in bulk. With decreasing the grain size to 2.2 nm, the 196.1 cm^{-1} peak disappears and the 396.1 and 516.1 cm^{-1} peaks individually blueshift to 402.4 and 519.5 cm^{-1}, while the 639.5 cm^{-1} peak blueshifts to 643.2 cm^{-1} first, and then redshifts to 632.1 cm^{-1}. The strongest peak at around 143 cm^{-1} is low frequency E_g mode and is expanded in Fig. 3 in order to be viewed clearly. As seen in Fig. 3, the 143 cm^{-1} mode blueshifts from 143.5 to 155.7 cm^{-1} and asymmetrically broadens from 7.6 to 35.3 cm^{-1} with a high frequency shoulder when the grain size decreases from 25.5 to 2.2 nm. Refs. [6–8] explained these variations of the 143 cm^{-1} mode with phonon confinement. The phonon confinement is involved in the breakdown of the phonon momentum selection rule, i.e., $q \neq 0$ phonons can be Raman active and the phonons from the whole Brillouin zone will contribute to Raman scattering. The weight of the off-centre phonons increase as the grain size decreases. The phonon dispersion causes an asymmetric broadening and the shift of the Raman peak. Usually, a Gaussian weighting func-

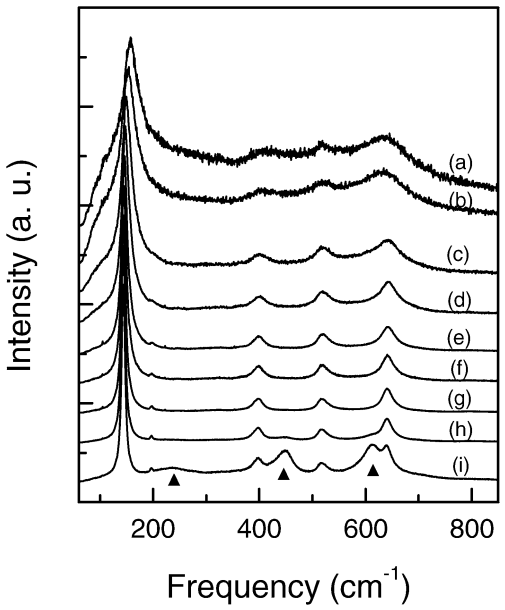

Fig. 2. Normalized Raman spectra from the TiO_2 nanocrystals at various particle sizes: (a) 2.2, (b) 2.5, (c) 3.2, (d) 5.1, (e) 7.8, (f) 12.7, (g) 14.6, (h) 20.4 and (i) 25.5 nm, respectively. Triangle ▲ indicates Raman peaks of rutile TiO_2.

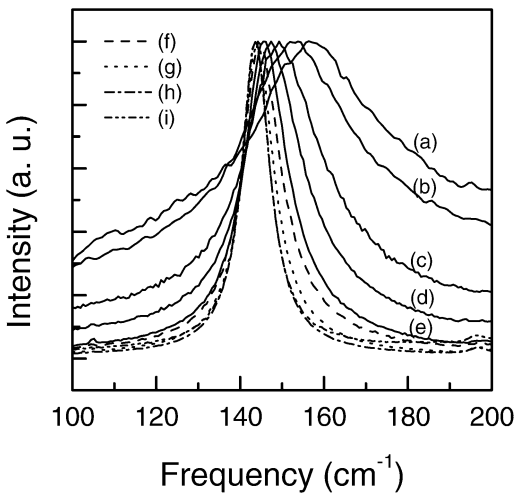

Fig. 3. An expanded view of the normalized Raman spectra of the 143 cm^{-1} mode. Curves (a), (b), (c), (d), (e), (f), (g), (h), (i) and (j) stand for samples of 2.2, 2.5, 3.2, 5.1, 7.8, 12.7, 14.6, 20.4 and 25.5 nm, respectively.

tion is used to model Raman scattering at wave vectors away from zone center. Several functions, such as sine, exponential, and Gaussian functions were discussed in the confinement [15]. The results fitting to Gaussian confinement was in good agreement with the experimental data. So Gaussian function was selected in the confinement discussion [5,15,16]

$$W(r, L) = \exp\left(-\alpha r^2/L^2\right), \tag{1}$$

where L is the diameter of a spherical grain and α is a coefficient to be found. Therefore, for a spherical grain of diameter L, the Raman intensity profile $I(\omega)$ is a superposition of the weighted Lorentzian contribution over the whole Brillouin zone [16]

$$I(\omega) \propto \sum_{i=1}^{2} \int_{BZ} \frac{\exp(-q^2L^2/2\alpha)}{[\omega - \omega_i(q)]^2 + (\Gamma_0/2)^2}\, d^3q, \tag{2}$$

where Γ_0 is the natural Raman full width at half maximum for bulk anatase, which is 7 cm^{-1} for the 143 cm^{-1} mode at room temperature [7]; q is the wave vector. The sum is carried over the two modes with $\omega_i(q)$, because the 143 cm^{-1} mode is a E_g mode, double degenerated at $q = 0$. Taking into account a spherical Brillouin zone with a diameter $2a/\pi$ and an isotropic dispersion, the calculation was performed by using a simple function, $\omega = \omega_0 + 20[1 - \cos(qa)]$, since there has been no phonon dispersion data provided for anatase phase. The calculated data in Ref. [8] well reproduced the phonon dispersion of the 143 cm^{-1} mode of the rutile instead of the anatase phase, and the size dependence of the bandwidth did not agree well with the experimental data. By using theoretical phonon dispersion curves of anatase [17], we calculate size dependences of frequency and bandwidth for the 143 cm^{-1} mode. The dispersion relationships for the low-frequency E_g mode in the anatase phase could be approximately expressed as

$$\omega_1 = \omega_0 + 28\left[1 - \cos(qa)\right] \tag{3}$$

and

$$\omega_2 = \omega_0 + 102\left[1 - \cos(qa)\right], \tag{4}$$

where $\omega_0 = 143$ cm^{-1} [5,18].

Both the frequency and bandwidth of the 143 cm^{-1} mode versus the particle size for the measured data from Fig. 3 and the calculated curves using Eq. (2) are shown in Fig. 4. It can be seen that when $\alpha = 25$, Raman frequency is the most close to the experimental data, but bandwidth deviates largely the experimental data, and for $\alpha = 35$ the situation is opposite to the case of $\alpha = 25$. When $\alpha = 30$, both frequency and bandwidth are close to the experimental data. Coefficient α takes different values under different models: $\alpha = 4$ in the Richter phonon-confinement model for Si nanocrystal [9], $\alpha = 8\pi^2$ in Campbell model for CdSe, c-BN and ZnO_2 nanocrystals [10,15,19,20], where phonons are strongly confined, thus only a small amount of atoms in the central part of the sphere can vibrate. In our case of $\alpha = 30$, the phonons are moderately confined and a large amount of atoms

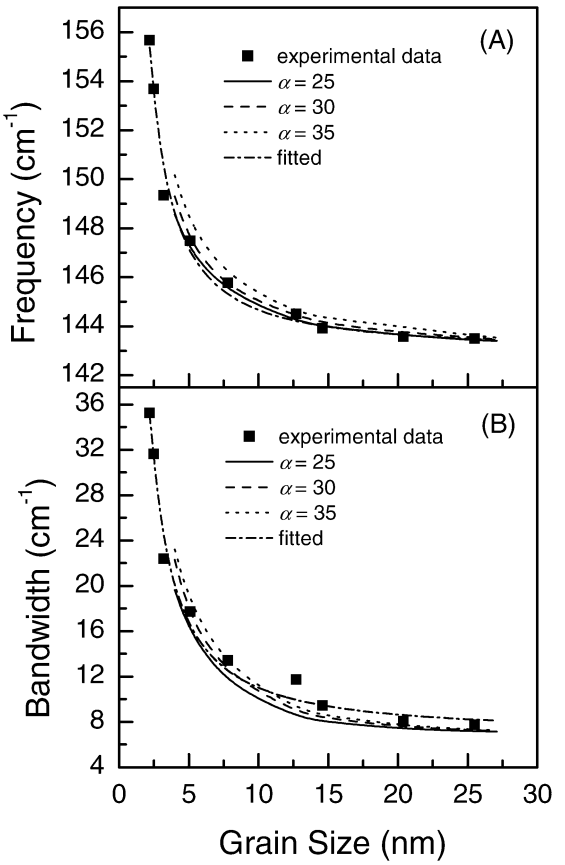

Fig. 4. Frequency (A) and bandwidth (B) of the 143 cm^{-1} mode versus particle size. Square ■ denotes experimental data. The solid, dashed and dotted curves stand for the calculated results on the basis of the phonon confinement model with $\alpha = 25$, $\alpha = 30$ and $\alpha = 35$, respectively. The dash-dotted curves are fitted to the empirical formulas.

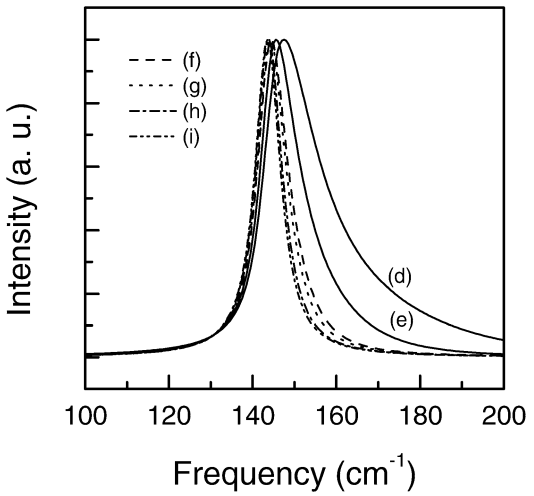

Fig. 5. Normalized Raman lineshape of the 143 cm^{-1} mode calculated on the base of the phonon confinement model at various particle sizes of (d) 5.1, (e) 7.8, (f) 12.7, (g) 14.6, (h) 20.4 and (i) 25.5 nm, respectively.

in the sphere center can vibrate. Fig. 5 shows the lineshapes of the 143 cm^{-1} mode calculated by using Eq. (2) at $\alpha = 30$ in the particle size range 5.1–25.5 nm. With decreasing the size, Raman mode shifts to higher frequency and asymmetrically broadens with a high-frequency shoulder, in good agreement with experimental results shown in Fig. 3. The calculated curves cannot extend below 4 nm, where a spherical Brillouin zone and isotropic dispersion curves are not hold, because the details of the shape of the Brillouin zone become critical [7]. Since our nanocrystal samples were prepared by a chemical method via annealing treatment, there may be oxygen deficient defect deviating from chemical stoichiometry. The defect also leads to changes of Raman frequency and bandwidth, because of shortening the correlation length of the phonons [6]. Since both the particle size and the defect confine spatial phonon correlation, it is difficult to distinguish pure size effects on Raman spectra from the defect effects. If the density of the defect is too high, the correlation length of the phonons is far smaller than the particle size, thus the density of the defect instead of the grain size mainly determines the Raman spectral change. This is the case presented in Ref. [5], where the changes observed in the Raman spectra were related to the oxygen stoichiometry and were not due to the size effects.

Two empirical formulas were used to describe correlations of both Raman frequency and bandwidth to nanocrystal size [16,21,22]

$$\omega(L) = \omega_0 + A(a/L)^{\gamma} \tag{5}$$

and

$$\Gamma(L) = \Gamma_0 + B(a/L)^{\gamma'}, \tag{6}$$

where $\omega(L)$ and $\Gamma(L)$ are individual Raman frequency and bandwidth in a nanocrystal with size L, parameters A, B, γ and γ' are relative to phonon confinement. By fitting the experimental data in Fig. 4(A) to Eq. (5), A and γ are equal to 127 cm^{-1} and 1.32; whereas by fitting the experimental data in Fig. 4(B) to Eq. (6), B and γ' are equal to 270 cm^{-1} and 1.29. The fitted results are also plotted as dash-dotted lines in Fig. 4(A) and (B), respectively. Empirical Raman-versus-size scaling exponent γ is equal to 1.0 for two-dimensional layered materials such as graphite, BN, and boehmite, to 1.5 for three-dimensional covalent network semiconductors, such as Si and GaAs [21]; and to about 1.5 and 1.0 for Si spheres and Si columns, respectively [22]. The values of γ and γ' are almost the same, so γ' is also taken as the Raman-versus-size scaling exponent. Considering the fact that the anatase crystal spans a three-dimensional network and the nanocrystals are spheres, the γ and γ' should be 1.5. However, both γ and γ' are to be equal to 1.3, the reason may stem from defects, such as oxygen vacancies in anatase TiO_2 nanocrystals.

Raman spectra from the 7.8 nm sized-sample at temperature 83–293 K are shown in Fig. 6. All the bandwidths decrease with decreasing temperature, which causes the 516 cm^{-1} Raman peak to be split two peaks at 515 cm^{-1} (A_{1g}) and 521 cm^{-1} (B_{1g}) at 83 K. This result is in agreement with result in Ref. [23], where 516 cm^{-1} peak to be split two peaks at 513 and 519 cm^{-1} at 73 K. The variations of the low-frequency mode with temperature are clearly shown in Fig. 6(B). The frequency and bandwidth equal 145.8 and 13.4 cm^{-1} at 293 K, and decrease to 141.0 and 7.3 cm^{-1}, respectively, as temperature decreases to 83 K. The temperature dependences of Raman frequency and bandwidth in a bulk semiconductor was attributed to the decay of the zone-center optical phonon via anharmonicity to two acoustic phonons of equal and opposite q-vectors so that they add up to zero [24]. In a nanocrystal, the q-vector selection rule may be

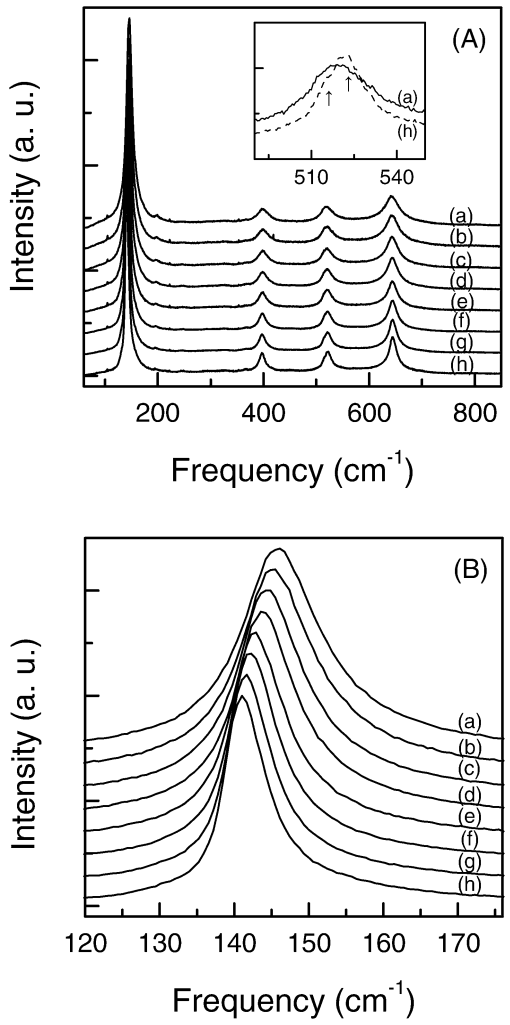

Fig. 6. Normalized Raman spectra (A) from the 7.8 nm sample at the temperatures of (a) 293, (b) 263, (c) 233, (d) 203, (e) 173, (f) 143, (g) 113 and (h) 83 K, respectively. Insert shows the split of the 516 cm^{-1} peak. An expanded view (B) of the 143 cm^{-1} mode shows temperature-dependences of both the frequency and bandwidth.

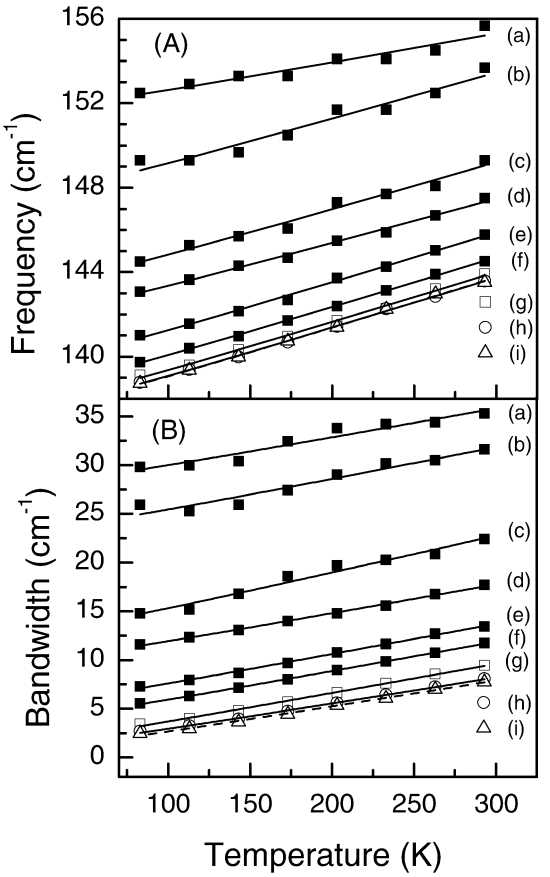

Fig. 7. Frequency (A) and bandwidth (B) of the 143 cm^{-1} mode versus temperature. Solid squares, open squares, circles and triangles correspond to experimental data at different particle sizes of (a) 2.2, (b) 2.5, (c) 3.2, (d) 5.1, (e) 7.8, (f) 12.7, (g) 14.6, (h) 20.4 and (i) 25.5 nm, respectively. The solid and dashed lines are fitted to Eqs. (7)–(10).

also relaxed, which enhances these three phonons coupling and changes the temperature dependences of Raman frequency and bandwidth at different grain sizes. The temperature dependence of Raman frequency is given by [24]

$$\omega(T) = \omega_1 + \Delta(T), \tag{7}$$

$$\Delta(T) = \omega_2\left[1 + \frac{2}{\exp(\hbar\omega_1/2KT) - 1}\right], \tag{8}$$

where ω_1 is the harmonic frequency. $\Delta(T)$ is the anharmonic term, which describe the contribution of three-phonon processes to Raman frequency, and ω_2 is a coefficient. The temperature dependence of Raman bandwidth is given by [11,24]

$$\Gamma(T) = \Gamma_1 + \Delta\Gamma(T), \tag{9}$$

$$\Delta\Gamma(T) = \Gamma_2\left[1 + \frac{2}{\exp(\hbar\omega_1/2KT) - 1}\right], \tag{10}$$

where $\Delta\Gamma(T)$ is from three-phonon coupling decay, additional width Γ_1 is due to broadening of phonon confinement. In bulk, Γ_1 equals zero and Γ_2 corresponds to the nature bandwidth at $T = 0$.

Table 1
Fit parameters for Raman frequency and linewidth

Size (nm)	2.2	2.5	3.2	5.1	7.8	12.7	14.6	20.4	25.5
ω_1 (cm^{-1})	151.11	146.74	142.38	141.07	138.67	137.51	136.79	136.50	136.46
ω_2 (cm^{-1})	0.75	1.17	1.15	1.07	1.19	1.18	1.17	1.18	1.18
Γ_1 (cm^{-1})	26.70	21.84	11.16	8.66	4.20	2.62	0.43	0.03	−0.21
Γ_2 (cm^{-1})	1.63	1.74	1.96	1.53	1.57	1.52	1.49	1.33	1.31

Both Raman frequency and bandwidth of the 143 cm^{-1} mode versus particle size at various temperatures are shown in Fig. 7(A) and (B), respectively. The experimental frequencies in Fig. 7(A) were fit to Eqs. (7) and (8) with ω_1 and ω_2 as the free parameters; whereas the experimental bandwidths in Fig. 6(B) were fit to Eqs. (9) and (10) with Γ_1 and Γ_2 as the free parameters and with the values of ω_1 obtained from the frequency fitting. The fitting parameters ω_1, ω_2, Γ_1 and Γ_2 were listed in Table 1. These fits were plotted as solid and dashed lines in Fig. 7. As seen in Table 1, the parameter ω_1 increases from 136.5 to 151.1 cm^{-1} as the size decreases from 25.5 to 2.2 nm. This change is attributed to the phonon confinement effect. The parameter ω_2 remains about 1.17 cm^{-1} as the size decreases from 25.5 to 2.5 nm, which suggests that the contribution of the three-phonon process to Raman frequency does not vary with the particle size. The parameter Γ_1 equals 0.03 cm^{-1} at the 20.4 nm sample, which is close to zero for the bulk, and then increases to 26.70 cm^{-1} when size decreases to 2.2 nm. This change is also ascribed to the phonon confinement effect. The parameter Γ_2 increases from 1.31 to 1.73 cm^{-1} when the grain size decreases from 25.5 to 2.5 nm. The increase in Γ_2 with decreasing grain size suggests that phonon decay via phonon coupling be faster in the smaller grain than that in the larger grain, i.e., the phonon coupling is increased in anatase TiO_2 nanocrystal. The results of Raman studies of nanocrystal Si films and CdSe nanocrystals in glass suggested stronger coupling in the nanodomains than in larger domains [9,10], but that of CeO_2 nanoparticles suggested no stronger coupling in nanoparticles than in larger-dimension material [11]. These different results may come from the differences of the phonon dispersion curves, confinement strength and the coefficients of anharmonic terms among these crystals. By the way, the brookite and amorphous TiO_2 in the 2.2 nm sample may cause the abnormal values of ω_2 and Γ_2; and the 143 cm^{-1} Raman peak from rutile phase in the 25.5 nm sample causes abnormal value of Γ_1.

4. Conclusion

Anatase TiO_2 nanocrystal with particle size range 2.2–25.5 nm were prepared using a hydrolysis process of tetrabutyl titanate under heat treatment. The low-frequency E_g mode shifts to higher frequency and asymmetrically broadens with a high-frequency shoulder as the particle size is decreased. The size dependence of the frequency, bandwidth and lineshape was calculated on the basis of the phonon confinement model with the theoretical phonon dispersion relationships. The results agree well with experimental data. Both Raman frequency and bandwidth versus the particle size L satisfy a $L^{-1.3}$ law. With decreasing the grain size the contribution of three-phonon anharmonic processes to the frequency keeps unchanged, and the rate of decay of phonon via three-phonon coupling is increased, manifesting enhancement of the phonon coupling in anatase TiO_2 nanocrystal.

Acknowledgements

This work was supported by the National Natural Science Foundation of China through Grants Nos. 10174034 and 10374047.

References

[1] L. Gleiter, Prog. Mater. Sci. 33 (1989) 223.
[2] B. O'Regan, M. Grätzel, Nature 353 (1991) 737.
[3] M. Koelsch, S. Cassaignon, J.F. Guillemoles, Thin Solid Films 403–404 (2000) 312.

[4] K. Peter, H. Wietasch, B. Peng, M. Thelakkat, Appl. Phys. A 79 (2004) 65.
[5] J.C. Parker, R.W. Siegel, Appl. Phys. Lett. 57 (1990) 943.
[6] Y. Iida, M. Furukawa, T. Aoki, T. Sakai, Appl. Spectrosc. 52 (1998) 673.
[7] D. Bersani, P.P. Lottici, X.Z. Ding, Appl. Phys. Lett. 72 (1998) 73.
[8] W.F. Zhang, Y.L. He, M.S. Zhang, Z. Yin, Q. Chen, J. Phys. D 33 (2000) 912.
[9] H. Richter, Z.P. Wang, L. Ley, Solid State Commun. 39 (1981) 625.
[10] A. Tanaka, S. Onari, T. Arai, Phys. Rev. B 45 (1992) 6587.
[11] J.E. Spanier, R.D. Robinson, F. Zhang, S.W. Chan, I.P. Herman, Phys. Rev. B 64 (2001) 245407.
[12] J.K. Burdett, T. Hughbanks, G.J. Miller, J.W. Richardson, J.V. Smith, J. Am. Chem. Soc. 109 (1987) 3639.
[13] G.A. Tompsett, G.A. Bowmaker, R.P. Cooney, J.B. Metson, K.A. Rodgers, J.M. Seakins, J. Raman Spectrosc. 26 (1995) 57.
[14] H. Chang, P.J. Huang, J. Raman Spectrosc. 29 (1998) 97.
[15] L.H. Campbell, P.M. Fauchet, Solid State Commun. 58 (1986) 739.
[16] J. Zi, K. Zhang, X. Xie, Phys. Rev. B 55 (1997) 9263.
[17] M. Mikami, S. Nakamura, Phys. Rev. B 66 (2002) 155213.
[18] R.J. Capwell, F. Spagnolo, M.A.D. Sessa, Appl. Spectrosc. 26 (1972) 537.
[19] T. Werninghaus, J. Hahn, F. Richter, D.R.T. Zahn, Appl. Phys. Lett. 70 (1997) 958.
[20] M. Rajalakshmi, A.K. Arora, J. Appl. Phys. 86 (2000) 2445.
[21] C.J. Doss, R. Zallen, Phys. Rev. B 48 (1993) 15626.
[22] J. Zi, X. Büscher, C. Falter, W. Ludwin, K. Zhang, X. Xie, Appl. Phys. Lett. 69 (1996) 200.
[23] T. Ohsaka, F. Izumi, Y. Fujiki, J. Raman Spectrosc. 7 (1978) 321.
[24] M. Balkanski, R.F. Wallis, E. Haro, Phys. Rev. B 28 (1983) 1928.